

Nonmonotonic Synaptic Excitation and Imbalanced Inhibition Underlying Cortical Intensity Tuning

Guangying K. Wu,^{1,4} Pingyang Li,¹ Huizhong W. Tao,^{1,3} and Li I. Zhang^{1,2,*}

¹Zilkha Neurogenetic Institute

²Department of Physiology and Biophysics

³Department of Ophthalmology

Keck School of Medicine

⁴Neuroscience Graduate Program

University of Southern California

Los Angeles, California 90033

Summary

Intensity-tuned neurons, characterized by their non-monotonic response-level function, may play important roles in the encoding of sound intensity-related information. The synaptic mechanisms underlying intensity tuning remain unclear. Here, *in vivo* whole-cell recordings in rat auditory cortex revealed that intensity-tuned neurons, mostly clustered in a posterior zone, receive imbalanced tone-evoked excitatory and inhibitory synaptic inputs. Excitatory inputs exhibit nonmonotonic intensity tuning, whereas with tone intensity increments, the temporally delayed inhibitory inputs increase monotonically in strength. In addition, this delay reduces with the increase of intensity, resulting in an enhanced suppression of excitation at high intensities and a significant sharpening of intensity tuning. In contrast, non-intensity-tuned neurons exhibit covaried excitatory and inhibitory inputs, and the relative time interval between them is stable with intensity increments, resulting in monotonic response-level function. Thus, cortical intensity tuning is primarily determined by excitatory inputs and shaped by cortical inhibition through a dynamic control of excitatory and inhibitory timing.

Introduction

Intensity-tuned neurons are characterized by their non-monotonic responses to tone intensities (Greenwood and Maruyama, 1965). Such neurons (also named non-monotonic neurons) have been observed along the central auditory pathway, including the cochlear nucleus (Greenwood and Maruyama, 1965; Young and Brownell, 1976), inferior colliculus (Aitkin, 1991; Kuwabara and Suga, 1993), medial geniculate body (Aitkin and Webster, 1972; Rouiller et al., 1983), and auditory cortex (Davies et al., 1956; Evans and Whitfield, 1964; Brugge et al., 1969; Schreiner et al., 1992; Phillips et al., 1995). The response properties of cortical intensity-tuned neurons (Phillips et al., 1995; Heil and Irvine, 1998) and their susceptibility to specific changes after training animals with a sound magnitude discrimination task (Polley et al., 2004, 2006) suggest that these neurons may play important roles in the encoding of sound loudness and

envelop transients. Because auditory nerve fibers, the inputs to the central auditory system, have monotonically increasing response-versus-intensity functions (Kiang et al., 1965), the generation of intensity tuning in the central auditory system must rely on neural inhibition to reduce activity preferentially at high intensities. Studies using extracellular recordings with two-tone masking paradigms (Suga and Manabe, 1982; Calford and Semple, 1995; Sutter and Loftus, 2003), with GABA receptor blockade (Faingold et al., 1991; Pollak and Park, 1993; Wang et al., 2002; Sivaramkrishnan et al., 2004), as well as using intracellular recordings (Ojima and Murakami, 2002) suggest that intensity tuning may be produced by the spatial and/or temporal interaction of the inhibition and excitation. However, without direct examination of sound-activated synaptic inputs in individual intensity-tuned neurons, the synaptic mechanisms or neuronal biophysical properties (D. Durstewitz and T.J. Sejnowski, 2000, Soc. Neurosci., abstract) that may underlie the nonmonotonic response-intensity function or the conversion from monotonic to nonmonotonic function remain elusive.

Recently, several studies on synaptic inputs underlying tone-evoked responses indicate that the frequency tuning and the frequency-intensity tonal receptive fields (TRFs) of cortical neurons are shaped by balanced excitatory and inhibitory synaptic inputs (Zhang et al., 2003; Wehr and Zador, 2003; Tan et al., 2004). This is evidenced by the covariation of the amplitudes of excitatory and inhibitory synaptic conductances evoked by the same tone stimulus (Zhang et al., 2003; Tan et al., 2004) and a relatively stable temporal interval between them (Wehr and Zador, 2003). However, those data were mostly acquired from the primary auditory cortex (A1) of rats, where the majority of neurons do not exhibit intensity tuning or exhibit weak tuning (Phillips and Kelly, 1989; Zhang et al., 2001; Doron et al., 2002; Polley et al., 2004, 2006). In the present study, using an *in vivo* whole-cell voltage-clamp recording technique, we examined the excitatory and inhibitory synaptic TRFs in two distinct classes of cortical neurons: intensity-tuned and non-intensity-tuned neurons. We quantified the amplitude and temporal relationship between the excitatory and inhibitory inputs evoked by tone stimuli of various intensities at characteristic frequencies (CFs) of the cells. Our data indicate that cortical intensity tuning is determined by the interplay between tone-evoked imbalanced excitatory and inhibitory synaptic inputs. In intensity-tuned neurons, excitatory inputs already exhibit intensity tuning, whereas the inhibitory inputs increase monotonically in their strength and quickly saturate with intensity increments. In addition, the temporal delay of inhibitory inputs relative to excitatory inputs is reduced with the increase of intensity, resulting in an enhanced suppression of excitation at high intensities and a significant sharpening of intensity tuning. These findings also imply that by controlling the relative timing of excitation and inhibition, synaptic circuits can achieve a *de novo* construction of representational properties.

*Correspondence: liizhang@usc.edu

Results

Distribution of Nonmonotonic Neurons in the Rat Auditory Cortex

To effectively investigate nonmonotonic neurons, we first determined the spatial distribution of such neurons in the adult rat auditory cortex by high-density mappings with multiunit extracellular recordings (100–180 sampling sites for each map, see [Experimental Procedures](#)). The frequency-intensity tonal receptive field for spike responses (spike TRF) was reconstructed for each recorded sampling site. The change of tone-evoked spike response in the function of tone intensity was examined at the characteristic frequency (CF), which is the frequency that the neuron is most sensitive to. As shown in an example auditory cortical map ([Figure 1A](#)), three major fields can be identified according to the tonotopic organization of frequency representations: the primary auditory cortex (A1), which exhibits a clear tonotopic gradient along the anterior-posterior axis; a small anterior auditory field (AAF), which exhibits a reversed tonotopic gradient compared to A1; and a ventral auditory field (VAF), which has an apparent dorsal-ventral CF gradient, consistent with previous reports ([Bao et al., 2003](#); [Kalatsky et al., 2005](#)). In these regions, the majority of sampling sites exhibited increased spike responses at high intensity levels ([Figure 1B](#), left). A typical monotonic function is shown after averaging spike response-level functions at CFs of 14 similar sites ([Figure 1B](#), right). Interestingly, sampling sites in a small posterior zone (named nonmonotonic auditory zone [NM]) located between A1 and VAF consistently exhibited nonmonotonic response-level functions, i.e., markedly reduced responses at high intensity levels ([Figure 1C](#)). In addition, the bandwidth of spike TRF at 30 dB above threshold (BW30) at those nonmonotonic sites was significantly narrower than at the monotonic sites ([Figure 1D](#)). In all of nine high-density mapping experiments, we observed a similar organization of frequency representation and the existence of a NM zone. Between sampling sites of the NM zone and those of the nearby A1 area that have similar CFs, no significant difference was observed in either the response onset latency (NM, 15.99 ± 0.32 ms [SEM]; A1, 15.72 ± 0.29 ms [SEM]; $p > 0.5$, ANOVA test) or the threshold of spike TRFs ($p > 0.5$, ANOVA test).

We used an intensity-tuning index to quantify the level of intensity tuning at CF. The index is defined as the ratio between the spike counts at the preferred intensity (with the highest level of response) and at 30 dB above the preferred intensity (or the highest intensity tested). Sampling sites with an index < 0.6 were considered to be strongly intensity tuned. In A1, about 5% of sampling sites exhibited strong intensity tuning, while in the NM zone, about 80% of sampling sites were strongly intensity tuned ([Figure 1E](#)). Our data are consistent with those from previous extracellular recordings ([Phillips and Kelly, 1989](#); [Doron et al., 2002](#); [Bao et al., 2003](#); [Polley et al., 2004, 2006](#)), which already suggest that nonmonotonic neurons are more abundant in the posterior part of the rat auditory cortex.

Excitatory and Inhibitory Synaptic Receptive Fields

To examine the synaptic mechanisms underlying intensity tuning of cortical neurons, we applied in vivo

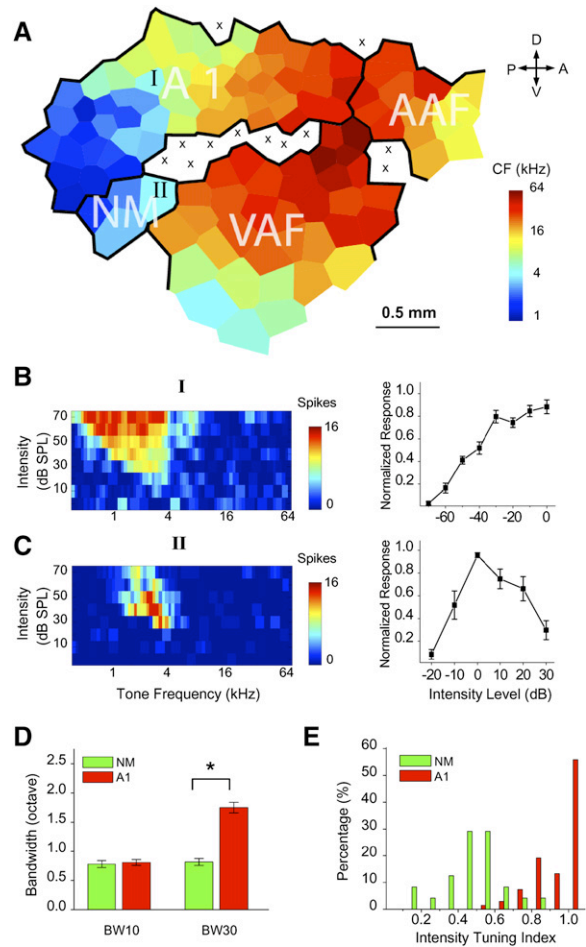


Figure 1. Multiunit Intensity Tuning in the Rat Auditory Cortex
 (A) An example map of frequency representation in the adult auditory cortex. The color indicates the characteristic frequency (CF) for the sampling site located in the center of each polygon. Polygons (Voronoi tessellations) were generated so that every point on the cortical surface was assumed to have the characteristics of its closest neighbors. A1, the primary auditory cortex; AAF, anterior auditory field; VAF, ventral auditory field; NM, nonmonotonic zone. A, anterior; D, dorsal; P, posterior; V, ventral. “x” indicates a sampling site that exhibited an intensity threshold of higher than 60 dB or no clear frequency tuning.
 (B and C) (Left) Tonal receptive field of spike responses (spike TRF) for a non-intensity-tuned site “I” and an intensity-tuned site “II,” as labeled in the map in (A). Color represents the number of spikes evoked by a tone stimulus. (Right) Normalized spike counts as a function of intensity level for CF tone stimuli. Intensity level “0” was set as where the highest spike rate was evoked. Data were from 14 randomly chosen non-intensity-tuned sampling sites in A1 near NM and nine intensity-tuned sites recorded within the NM zone, respectively. Error bar, SEM.
 (D) Bandwidths at 10 dB (BW10) and 30 dB (BW30) above intensity threshold measured for A1 units and NM units. Error bar, SEM. * indicates significant difference, $p < 0.03$, ANOVA test.
 (E) Distribution of intensity-tuning indices of A1 (red, $n = 65$) and NM (green, $n = 24$) units.

whole-cell voltage-clamp recordings (see [Experimental Procedures](#)) to neurons in A1 and the NM zone. By voltage-clamping the cell’s membrane potential at -70 mV and 0 mV, the reversal potentials for GABA_A receptor-mediated Cl⁻ currents and glutamate

receptor-mediated excitatory currents, respectively, we obtained TRFs for both excitatory and inhibitory inputs in the recorded cell. Synaptic TRFs for an example cell in the NM zone were shown in [Figures 2A and 2B](#), and for a cell in A1 were shown in [Figures 2C and 2D](#). Linear current-voltage relationship (I-V curve) was observed for the recorded synaptic currents evoked by CF tones at 70 dB SPL ([Figure 2E](#)). The derived reversal potential for the early component of these currents (mainly excitatory) was 0 ± 4 mV (SD), close to the known reversal potential for glutamatergic currents. These data suggest that, under our voltage-clamp recording conditions, those synaptic inputs that contributed to the recorded tone-evoked currents were detected with a reasonable accuracy (see [Experimental Procedures](#)). The excitatory and inhibitory synaptic TRFs obtained from voltage-clamp experiments provide a basis for determining the synaptic mechanisms underlying the intensity-tuning properties of cortical neurons.

Intensity tuning is usually defined at CFs of cortical neurons according to their spike responses ([Schreiner et al., 1992](#); [Phillips et al., 1995](#); [Heil and Irvine, 1998](#); [Polley et al., 2004](#)). Because synaptic TRF usually exhibits a lower intensity threshold and is broader than the spike TRF of the same cell ([Tan et al., 2004](#)), to be consistent with previous studies, the CF of the cell was estimated according to the TRF of membrane potential responses, which were derived from the excitatory and inhibitory synaptic conductances evoked by each tonal stimulus (see [Experimental Procedures](#)). Based on the resting membrane potential of the cell and the threshold for spike generation (-45 mV; [Tan et al., 2004](#)), the frequency-intensity responsive area for spike responses was then estimated ([Figures 2G and 2H](#), hatched area). The CF was defined as the frequency at the threshold intensity of the spike TRF. For the example cell recorded from the NM zone ([Figure 2G](#)), the intensity threshold was estimated to be 20 dB SPL and the CF to be 2.14 kHz \pm 0.1 octaves. At this CF, the membrane potential response changed nonmonotonically with the increase of intensity, with the strongest response evoked at an intensity level close to the intensity threshold ([Figure 2G](#)), suggesting that this cell represents a typical intensity-tuned neuron. In contrast, for the example cell recorded from A1 ([Figure 2H](#)), the derived membrane potential response at the CF changed monotonically with intensity increments, consistent with multiunit recording results for monotonic sites ([Figure 1B](#)). In addition, although both the intensity-tuned and untuned neurons exhibited broad synaptic TRFs, the spike TRF of the intensity-tuned neuron was much smaller ([Figures 2G](#), hatched area) and became circumscribed, consistent with multiunit recording results for many nonmonotonic sites ([Figure 1C](#)). The response-intensity functions of calculated membrane-potential responses correlated well with those of directly recorded membrane-potential responses, as shown in five recorded neurons in which both voltage-clamp and current-clamp recordings were obtained ([Figure 3](#)). Thus, by integrating excitatory and inhibitory synaptic conductances, we were able to determine the monotonic or nonmonotonic response properties of the neurons.

Nonmonotonic Excitation and Imbalanced Inhibition Underlying Intensity Tuning

We next determined the relative contribution of excitatory and inhibitory inputs to intensity tuning of cortical cells by examining the amplitude of CF tone-evoked excitatory and inhibitory synaptic conductances as a function of intensity level, i.e., the amplitude-level function. In both the intensity-tuned and untuned neurons, the excitatory and inhibitory synaptic TRFs exhibited an identical shape ([Figures 2A and 2B and 2C and 2D](#)). However, for the intensity-tuned neuron, there was a difference in the amplitude-level function between excitatory and inhibitory conductances. It appeared that the amplitudes of excitatory currents evoked by CF tones were smaller at high intensity levels ([Figure 2A](#), shaded column), while those of inhibitory currents remained more or less similar ([Figure 2B](#), shaded column). To quantify this phenomenon, after determining the CF, the excitatory and inhibitory synaptic conductances evoked by repeated CF tones were averaged for various intensities. The same tone stimulus evoked relatively consistent synaptic responses with small variations in amplitude (SD < 5% mean amplitude) and small jitters in response latency (SD < 0.3 ms; [Figure 2F](#)). As shown in [Figure 4A](#) for the intensity-tuned neuron, the amplitude of the averaged excitatory conductance changed nonmonotonically, with the peak amplitude evoked at the threshold intensity (20 dB SPL). The amplitude of the inhibitory conductance instead increased monotonically with the increase of intensity. Thus, the excitatory and inhibitory inputs were imbalanced in this intensity-tuned neuron, similar as a recent observation reported online ([Tan et al., 2006](#)). In contrast, for the example non-intensity-tuned neuron ([Figure 4B](#)), excitatory and inhibitory inputs exhibited similar monotonic tuning curves, consistent with the previous findings of balanced excitatory and inhibitory inputs that underlie the tone-evoked responses of A1 neurons ([Zhang et al., 2003](#); [Wehr and Zador, 2003](#); [Tan et al., 2004](#)). These data suggest that the intensity tuning of the cortical neuron is primarily inherited from the nonmonotonic excitatory inputs.

Inhibitory Contribution to Nonmonotonic Intensity Tuning

To determine whether the monotonic inhibitory inputs contribute to intensity tuning, we compared the intensity-tuning curves of membrane-potential responses derived by considering excitatory conductances only and by integrating excitatory and inhibitory conductances. As shown in [Figure 4C](#), for the same intensity-tuned neuron, excitatory conductances alone cannot fully account for the intensity-tuning curve, because the amplitude of membrane potential changes (PSPs) derived from excitatory conductances alone was reduced from the peak by only about 25% at the highest intensity ([Figure 4C](#), filled triangles), and even the weakest excitatory input (at 70 dB SPL) was capable of triggering spikes. Integrating the inhibitory conductances (averaged value) not only reduced the amplitude of membrane-potential responses in general but also significantly enhanced the intensity tuning, as indicated by a steeper reduction in the membrane-potential responses with intensity increments ([Figure 4C](#), filled squares). At the highest intensity, the PSP was reduced

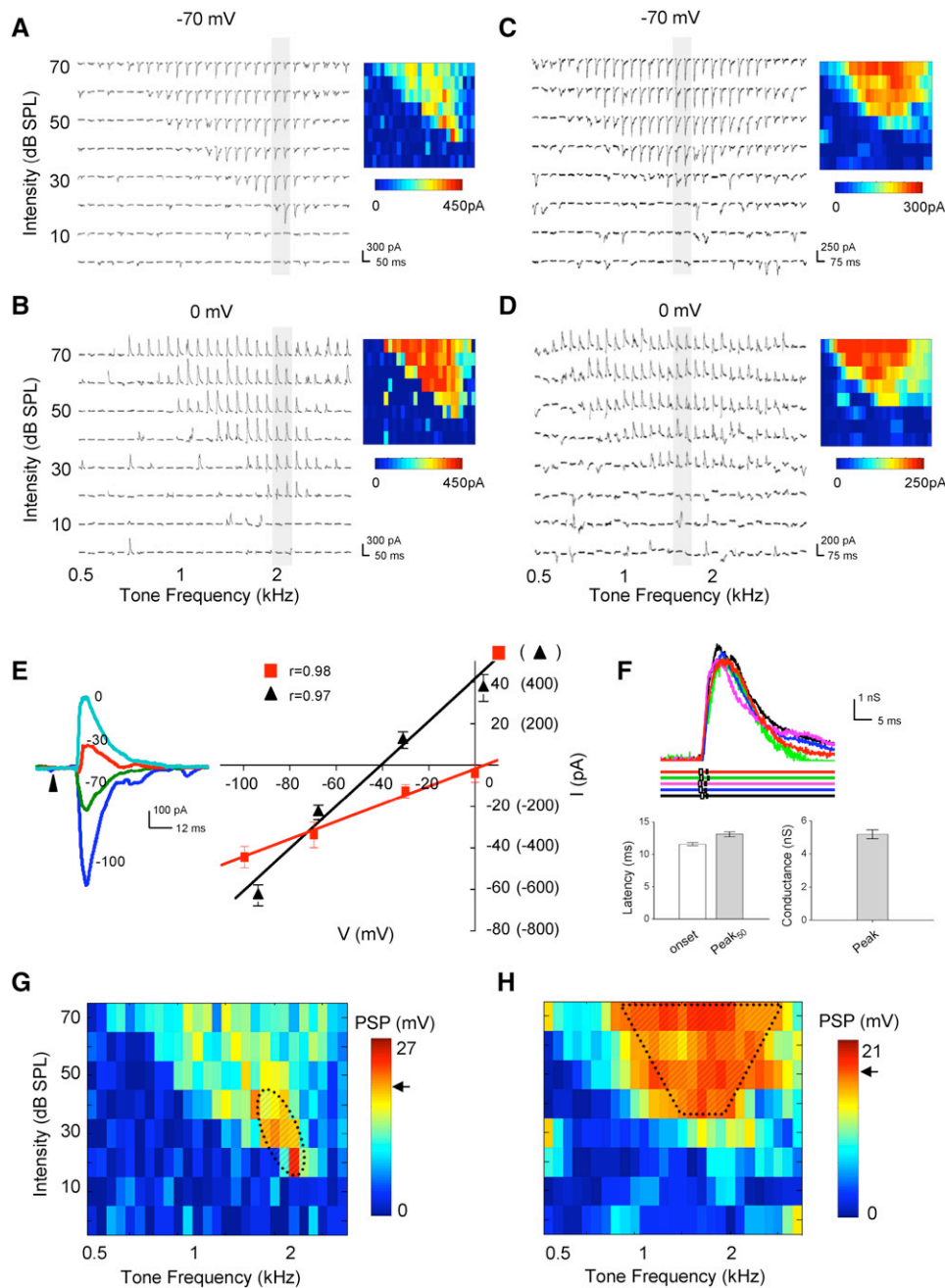


Figure 2. Synaptic TRFs of Intensity-Tuned and Non-Intensity-Tuned Neurons

(A and B) An example intensity-tuned neuron recorded from the NM zone. TRFs of synaptic currents evoked by pure tone stimuli at various frequencies and intensities were obtained, with the neuron clamped at -70 mV (A) and 0 mV (B), respectively. The color maps on the right indicate the amplitudes of individual synaptic currents.

(C and D) An example non-intensity-tuned neuron recorded from A1. Data are presented in the same manner as in (A) and (B).

(E) (Left) Synaptic currents (average of five repeats) evoked by a CF tone at 70 dB, recorded at different holding potentials from the same neuron shown in (A) and (B). Arrowhead indicates the onset of tone stimuli. (Right) I-V curves for synaptic currents averaged within 0 – 1 ms (red) and 20 – 22.5 ms (black) windows after the response onsets. Error bar, SEM.

(F) Jitters of responses to repeated stimuli (70 dB CF tone). (Upper panel) Small white box on the color line indicates the time point at the onset of the response of the same color shown on top; small black bar indicates the time point at 50% peak response. (Lower panel) Average latencies and peak conductance. Error bar, SD.

(G) TRF of peak membrane-potential responses derived from each pair of synaptic inputs recorded at -70 mV (A) and 0 mV (B). Color represents the postsynaptic potential change in millivolts. The resting membrane potential of the cell was -65 mV. Arrow indicates the spike threshold for required membrane-potential change. Hatched area represents the estimated spike TRF and roughly covers all the stimuli that could trigger suprathreshold responses. Note that the estimated spike TRF of this cell is circumscribed.

(H) TRF of peak membrane-potential responses derived for the cell shown in (C) and (D). The resting membrane potential of this cell was -61 mV.

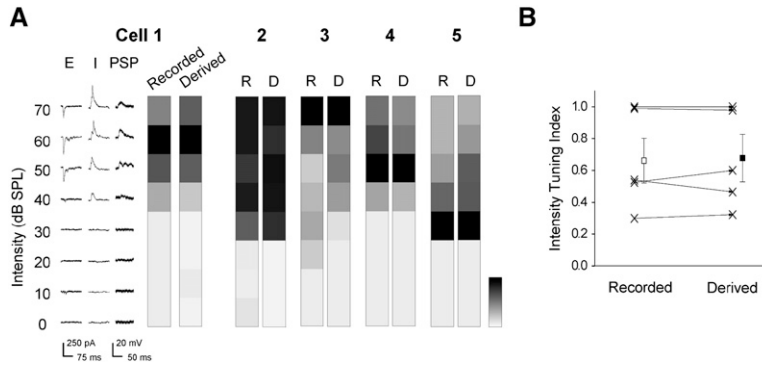


Figure 3. Intensity Tuning of Recorded and Derived Membrane-Potential Responses

(A) (Left) Average excitatory (recorded at -70 mV) and inhibitory (recorded at 0 mV) synaptic currents and recorded membrane-potential changes (PSPs) at CF (1.07 kHz) and 0 – 70 dB intensities for cell 1. Note that due to QX-314, which was included intracellularly, spikes of the recorded neuron were blocked. (Right) Maps in grayscale depict the peak amplitudes of the recorded PSPs (Recorded, “R”) and the derived PSPs (Derived, “D”) for cell 1 and another four cells. Monotonic neurons, cell 2, 3; nonmonotonic neurons, cell 1, 4, 5. Grayscale bar: white, 0 mV; black, maximal value, 18 mV, 22 mV for cell 1; 15 mV, 17 mV for cell 2; 17 mV, 20 mV for cell 3; 15 mV, 16 mV for cell 4; 26 mV, 32 mV for cell 5. (B) Intensity-tuning indices for the recorded PSPs and derived PSPs from the same cell. Squares indicate the average. Error bar, SEM. There is no significant difference between these two groups: $p > 0.9$, paired t test.

by 75% from the peak, leaving only a narrow range of intensities (20 – 30 dB SPL) at which spikes can be generated. In comparison, for the non-intensity-tuned neuron, the inhibitory conductances only scaled down the membrane-potential responses without changing the shape of the tuning curve (Figures 4B and 4D). These results indicate that cortical inhibition is actively involved in shaping the intensity tuning of cortical neurons.

Temporal Shaping of Nonmonotonic Intensity Tuning by Synaptic Inhibition

Cortical inhibitory inputs can shape spike responses through their temporal interaction with excitatory inputs (Zhang et al., 2003; Wehr and Zador, 2003; Zhu et al., 2004). For example, cortical synaptic inhibition enhances the direction selectivity of cortical responses to frequency-modulated sound sweeps through a larger

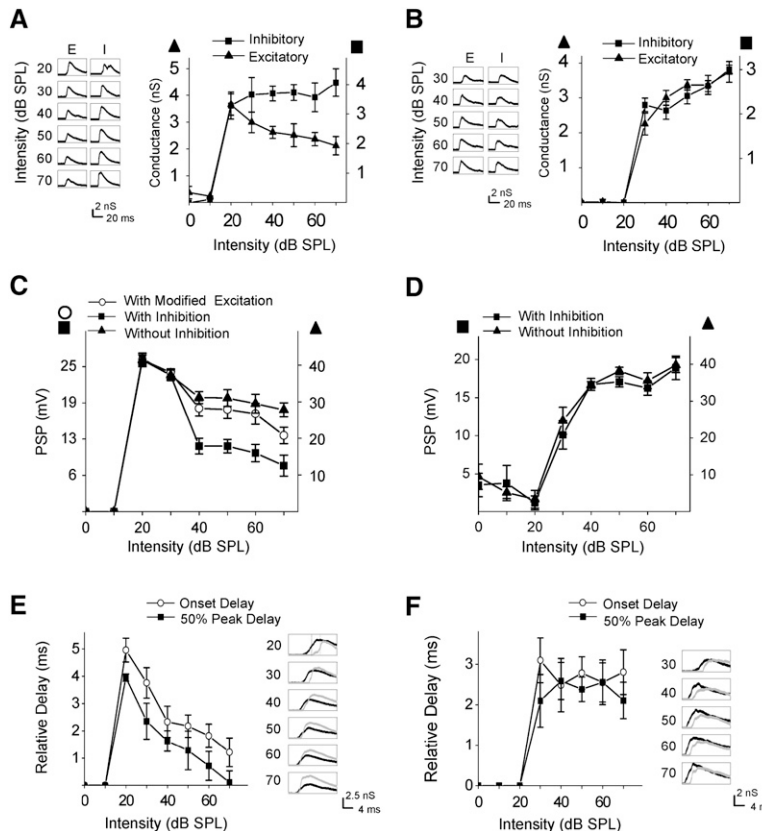


Figure 4. Intensity Tuning of Synaptic Conductances Evoked by CF Tones

(A) (Left) Traces of average excitatory (“E”) and inhibitory (“I”) synaptic conductances responding to different CF tone intensities for the intensity-tuned neuron shown in Figures 2A, 2B, and 2G. Traces are average from five repetitions. (Right) Average peak excitatory and inhibitory conductances as a function of tone intensity. Error bar, SEM. (C) Derived membrane-potential changes from (A) as a function of tone intensity, by considering excitatory inputs only (filled triangle), by integrating excitatory and inhibitory inputs (filled square), or by integrating inhibitory inputs and modified excitatory inputs (open circle). The excitatory inputs were modified as such that amplitudes of all responses to tones above 20 dB were scaled to that at 20 dB, which was the peak value. The error bars (SEM) were generated for derived PSPs by randomly pairing excitatory input and inhibitory input in different repeats. (E) Left column, 50% peak delay (filled square) and onset delay (open circle) of inhibitory conductances relative to the associated excitatory conductances, plotted as a function of tone intensity. 50% peak delays were extracted from waveforms at half-maximal amplitude (inhibition minus excitation). Error bars were the summation of the variations (SD) in the timing of excitatory and inhibitory inputs. Right column, pairs of average excitatory (black) and inhibitory (gray) synaptic conductances from (A) plotted at a higher temporal resolution. (B, D, and F) Same presentation as in (A), (C), and (E), but for the non-intensity-tuned neuron shown in Figures 2C, 2D, and 2H.

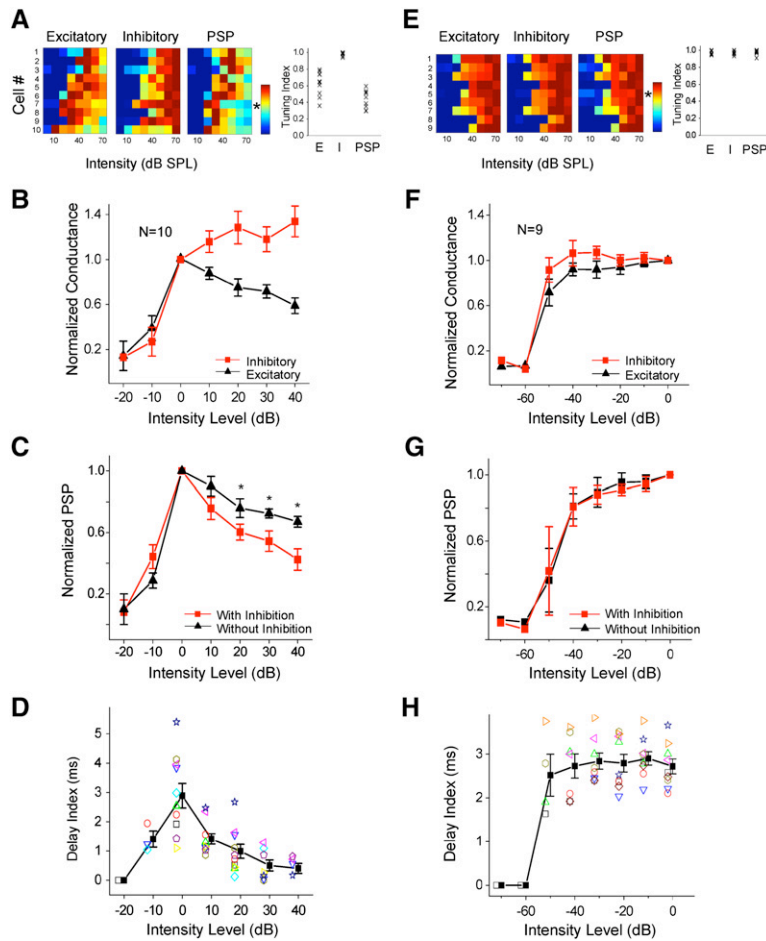


Figure 5. Summary for Intensity-Tuned (Non-monotonic) and Untuned Neurons

(A) A group of intensity-tuned neurons. Color maps depict average peak excitatory and inhibitory conductances (from three to five repetitions) and membrane potential changes at 0–70 dB intensities of CF tones for each of ten recorded NM neurons. Scale bar: dark blue, 0; dark red, maximal value: from cell 1 to cell 10, 4 nS, 3 nS, 5 nS, 3 nS, 4 nS, 5 nS, 4 nS, 7 nS, 6 nS, 2 nS for excitatory conductance; 5 nS, 2 nS, 6 nS, 2 nS, 3 nS, 7 nS, 4 nS, 5 nS, 6 nS, 2 nS for inhibitory conductance; 16 mV, 15 mV, 16 mV, 21 mV, 33 mV, 18 mV, 28 mV, 17 mV, 14 mV, 23 mV for PSP. (Right) Scatter plot of intensity-tuning indices for excitatory conductance, inhibitory conductance, and PSP of each recorded neuron. (B) Normalized evoked synaptic conductances of intensity-tuned neurons recorded from the NM zone, as a function of relative intensity of CF tones. Black triangle, excitatory; red square, inhibitory. Error bar, SEM, in this figure.

(C) Normalized membrane-potential changes, as a function of relative intensity. Red square, with consideration of inhibition; black triangle, without consideration of inhibition. * $p < 0.03$, paired t test.

(D) Relative delay of inhibition, as a function of relative intensity. Data from the same cell are represented by the same color and symbol. Black squares are average results. Error bar, SEM.

(E–H) Same as (A)–(D), respectively, but for the group of non-intensity-tuned neurons ($n = 9$) recorded in A1. Scale bar for the color maps in (E): dark blue, 0; dark red, maximal value: 2 nS, 5 nS, 2 nS, 4 nS, 4 nS, 3 nS, 4 nS, 4 nS, 2 nS for excitatory conductance; 2 nS, 3 nS, 2 nS, 2 nS, 3 nS, 3 nS, 5 nS, 5 nS, 4 nS for inhibitory conductance; 22 mV, 31 mV, 18 mV, 26 mV, 21 mV, 19 mV, 24 mV, 28 mV, 16 mV for PSP.

suppression of synaptic excitation under stimuli of non-preferred direction than of preferred direction (Zhang et al., 2003). This is achieved by a larger temporal overlap between excitatory and inhibitory inputs evoked by nonpreferred stimuli, due to an asymmetric integration of inputs sequentially activated by sound sweeps (Zhang et al., 2003). Here we examined the level of temporal overlap between CF tone-evoked excitatory and inhibitory conductances at different intensities. The average excitatory and inhibitory conductances evoked by the same tone stimulus were plotted together (Figure 4E, right). Consistent with the previous results (Zhang et al., 2003; Wehr and Zador, 2003; Tan et al., 2004), inhibitory inputs followed the excitatory inputs with a brief temporal delay. To quantify the relative delay of the inhibitory inputs, a delay index was used, which was defined as the interval between the time points at which 50% peak amplitude was reached in the rising phase of the average excitatory and inhibitory conductance traces (inhibition minus excitation; Wehr and Zador, 2003). Interestingly, for the example intensity-tuned neuron, the delay index reduced with the increase of intensity (Figure 4E, left, filled squares), whereas for the example non-intensity-tuned neuron, it remained more or less the same across different intensity levels

(Figure 4F). We also measured the difference in the onset latencies of excitatory and inhibitory inputs, which were defined as the time points at which the amplitude of evoked conductance became larger than three times the standard deviation of the baseline fluctuation. The result was consistent with the measurement of delay indices (Figures 4E and 4F, open circles). The reduced relative delay of inhibition as intensity goes higher leads to an increased temporal overlap between excitatory and inhibitory inputs, and thus a larger suppression of tone-evoked excitation at high intensities. Surprisingly, such nonmonotonic change of inhibitory delay can be sufficient for the generation of intensity tuning. This is demonstrated by the nonmonotonic tuning of membrane-potential responses achieved even after removing the nonmonotonicity of the excitatory inputs by keeping their amplitudes always at the peak value (at 20 dB) (Figure 4C, open circles).

Synaptic Mechanisms for Cortical Intensity Tuning

A total of 13 intensity-tuned neurons were recorded from the NM zone. In ten of them, complete excitatory and inhibitory synaptic TRFs were obtained (Figure 5A). Data from these neurons were summarized. Here, the intensity-tuning index was defined as the ratio between the

response amplitudes (either synaptic conductances or membrane-potential changes) at the preferred intensity and at the highest intensity tested. All of these neurons had an intensity-tuning index <0.6 for their derived membrane-potential responses (PSPs), and were tuned to intensities close to their intensity thresholds (Figures 5A and 5B). In all of them, excitatory inputs were clearly tuned, as indicated by their intensity-tuning indices (<0.8 ; Figure 5A), and their nonmonotonically changing amplitudes with intensity increments (Figure 5B). In contrast, inhibitory inputs were not tuned to intensity and their monotonically changing amplitudes quickly saturated (Figures 5A and 5B). Consistent among all the intensity-tuned neurons, cortical inhibition played an important role in sharpening the intensity tuning, as indicated by the significant difference between the tuning curves obtained with excitatory inputs alone and with both inputs taken into account (Figure 5C). This effect can be largely attributed to the significantly reduced temporal delay of inhibitory inputs relative to the excitatory inputs at high intensities (Figure 5D). As a comparison, for nine non-intensity-tuned neurons recorded from A1, excitatory and inhibitory inputs exhibited similar monotonic changes in the amplitude (Figures 5E and 5F). The intensity-tuning indices for both the synaptic conductances and derived PSPs were larger than 0.9. The inhibitory delay did not exhibit an intensity-dependent change (Figure 5H). The end result is that synaptic inhibition in non-intensity-tuned neurons only scales down the membrane-potential responses, without changing the shape of the intensity-tuning curve (Figure 5G). Taken together, although the extent to which synaptic excitation is thalamic or cortical in origin cannot be inferred from our data, we conclude that intensity tuning of cortical neurons is primarily inherited from their excitatory inputs relayed from intensity-tuned neurons and is further enhanced by cortical inhibitory inputs.

Discussion

Nonmonotonic Neurons in the Auditory Cortex

The distribution of nonmonotonic neurons has been extensively studied in the cat auditory cortex with extracellular recording methods. Nonmonotonic neurons have been observed throughout cat A1: besides mildly tuned units, about 25% of sampling units exhibit strong intensity tuning with the firing rate reduced by $>50\%$ at high intensities compared to that at the preferred intensity (Heil et al., 1994; Sutter and Schreiner, 1995). In addition, in the posterior auditory field (PAF or Field P), roughly 80% of the neurons exhibit intensity tuning, and about 40% of them show circumscribed spike TRFs (Heil and Irvine, 1998; Kitzes and Hollrigel, 1996; Phillips and Orman, 1984). Despite the difference in location, experimental data suggested that common neural mechanisms may underlie the nonmonotonic response-level function of both A1 and PAF neurons (Sutter and Loftus, 2003; Ojima and Murakami, 2002). In the present study of rat auditory cortex, both the location and the response properties of neurons of the NM zone (more than 80% of neurons exhibiting nonmonotonicity) are very similar to those of Field P in the cat auditory cortex (Read et al., 2002). However, in A1 only about 5% of neu-

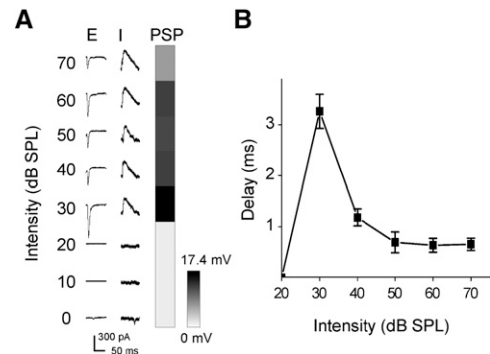


Figure 6. An A1 Nonmonotonic Cell

(A) A cell recorded in A1 exhibited similar characteristics of intensity tuning as neurons in the NM zone. Average excitatory (with cell clamped at -70 mV) and inhibitory (clamped at 0 mV) synaptic responses, and peak amplitudes of derived membrane-potential changes at CF (2.14 kHz) and 0–70 dB intensities are shown. The amplitudes of excitatory inputs as well as the membrane-potential responses exhibit nonmonotonic tuning, while those of inhibitory inputs change monotonically with intensity increments.

(B) The relative onset delays of inhibitory inputs at various intensities for the same cell in (A). Error bar, SD. Note that this cell is not included for summary in Figure 5.

rons are significantly intensity tuned, with intensity-tuning indices <0.6 (Figure 1E). Because of the sparseness of nonmonotonic cells in rat A1, only one such cell was recorded in our experiment (Figures 6A and 6B). In this cell, the tuning curves for excitatory and inhibitory inputs were similar to those in NM neurons, suggesting that the synaptic mechanisms revealed in this study may represent common mechanisms for nonmonotonic response-level functions. As discussed below, these mechanisms can also account for neural models proposed for nonmonotonic cells in cat auditory cortex.

Previous studies indicate that major forms of social vocalization in rats are ultrasonic (16–64 kHz), also termed 22 kHz calls (Sales and Pye, 1974; Nyby and Whitney, 1978; Kaltwasser, 1990; Brudzynski et al., 1993; Brudzynski and Pniak, 2002; Hashimoto et al., 2004). This is consistent with the relatively broad cortical representation of high frequencies in the rat auditory cortex (Figure 1A). Interestingly, it appears that intensities of low-frequency sounds are more broadly represented since neurons in the NM zone normally have CFs of lower than 8 kHz (Figure 1 and data not shown). While intensities of high-frequency sounds could be represented by sparsely distributed nonmonotonic cells in A1 (Figure 1E; Zhang et al., 2001; Bao et al., 2003; Polley et al., 2004, 2006), the relationship between the distribution of nonmonotonic cortical cells and the ability of rats to discriminate intensities of sounds at various frequencies remains to be investigated.

Nonmonotonic Excitation Primarily Determines Intensity Tuning

Previously, lateral inhibition has been proposed to be responsible for producing intensity tuning at higher levels of the auditory system (Shamma, 1985; Suga and Manabe, 1982; Phillips et al., 1995; Calford and Semple, 1995; Sutter and Loftus, 2003). This model has been supported by extracellular recording experiments using

forward-masking or simultaneous two-tone-masking paradigms (Suga and Manabe, 1982; Calford and Semple, 1995; Sutter and Loftus, 2003). These studies suggested that the intensity tunings of excitatory and suppressive domains were negatively correlated and that inhibitory sidebands could be involved in intensity tuning. However, due to the nature of the masking protocol, lateral suppressive domains may reflect complex temporal interaction between various synaptic inputs evoked by the testing sounds and may not reflect the frequency-intensity range of inhibitory synaptic inputs per se. By deriving excitatory and inhibitory synaptic conductances, we demonstrated that in nonmonotonic neurons inhibitory inputs always follow excitatory inputs evoked by the same tone stimulus, indicating that a pure inhibition domain in the TRF is not necessary for generating intensity tuning. Nevertheless, the nonmonotonic tuning of excitatory inputs and the monotonic tuning of inhibitory inputs agree with the negatively correlated excitation and inhibition suggested in previous studies. Since both intensity-tuned and untuned cortical neurons have monotonic inhibition, the intensity tuning is thus primarily determined by nonmonotonic excitatory inputs.

Temporal Shaping of Intensity Tuning by Inhibitory Inputs

The proposed lateral inhibition underlying the intensity tuning may reflect in part differential temporal interaction between excitatory and inhibitory synaptic inputs at various intensities. The temporal shaping effect of inhibitory inputs has recently been suggested in an intracellular study, which examined tone-evoked membrane depolarization and hyperpolarization, and showed that the onset latency of hyperpolarization became shorter as sound intensity increased, resulting in a shortening of the duration of the preceding depolarization (Ojima and Murakami, 2002). Because the membrane-potential response is determined by the temporal integration of both excitatory and inhibitory inputs, the property of each input cannot be directly inferred, e.g., the onset of hyperpolarization cannot be simply considered as the onset of inhibitory inputs. By dissecting tone-evoked pure excitatory and inhibitory synaptic conductances in well-defined intensity-tuned neurons, our findings extended the previous observations. Instead of simply scaling down the membrane-potential responses (Wehr and Zador, 2003; Tan et al., 2004), inhibitory inputs have significantly sharpened intensity tuning, an effect that can be largely attributed to a nonmonotonic tuning of the relative delay of these inputs.

How does nonmonotonic tuning of inhibitory delay arise? Although the absolute onset latencies of both excitatory and inhibitory inputs decrease with intensity increments in both intensity-tuned and untuned neurons (Heil, 2004; Figures 4A and 4B), the relative delay of inhibitory inputs becomes shorter at high intensities only in intensity-tuned neurons. We speculate that this change of temporal delay can be partially attributed to an intrinsic synaptic mechanism, i.e., the integration time to bring the neuron to firing threshold is determined by the slope and amplitude of the evoked excitatory postsynaptic potential (PSP) according to the integrate-and-fire model. In our recorded neurons, stronger

PSPs are accompanied by stronger excitatory conductances with steeper slopes (Figures 4A and 4B), indicating that a monotonic increase in PSPs will result in a monotonic reduction in the integration time for the initial spike and vice versa. If this holds for earlier stages of the auditory pathway, the nonmonotonic excitatory inputs to the cortical intensity-tuned neurons will inherit a longer integration time at high intensities, and the monotonic inhibitory inputs will inherit a shorter integration time instead, resulting in a shortening of the relative time interval between the two inputs. It is possible that the latter effect alone could be exploited by a neural network to convert a monotonic tuning curve to nonmonotonic. The implication of our results is that by controlling the relative timing of excitation and inhibition, synaptic circuits can achieve a de novo construction of representational properties.

Potential Synaptic Circuits Underlying Nonmonotonic Neurons

Synaptic circuits underlying nonmonotonic cortical neurons appear to be different from monotonic cells. Synaptic TRFs of A1 monotonic neurons are marked by covaried tone-evoked excitatory and inhibitory synaptic inputs (Zhang et al., 2003; Wehr and Zador, 2003; Tan et al., 2004). This suggests a feedforward inhibition circuit associated with A1 neurons, in which the presynaptic GABAergic neurons may be innervated by the same set of thalamocortical afferents as the recorded A1 cell, similar as previously proposed for other sensory cortices (Miller et al., 2001). In the present study, as recordings were made in the major thalamo-recipient layers of the auditory cortex, the noncovaried excitatory and inhibitory inputs in the intensity-tuned neurons suggest that the inhibitory inputs are from cortical GABAergic neurons innervated by a group of monotonic neurons in the thalamus, whereas excitatory inputs are likely mainly from thalamic nonmonotonic neurons. The latter is supported by the existence of nonmonotonic neurons in the medial geniculate body (Aitkin and Webster, 1972) and by the evidence that CF tone-evoked excitation can be largely attributed to thalamocortical inputs (Cruikshank et al., 2002; Kaur et al., 2004).

Finally, in this study, we followed previous studies (Schreiner et al., 1992; Phillips et al., 1995; Heil and Irvine, 1998; Polley et al., 2004) in characterizing responses to pure tones of various intensities at the CFs of the recorded neurons. Under more complex stimuli, the spike response-intensity function of intensity-tuned neurons will be complicated by the spectrotemporal integration of synaptic inputs activated at different frequencies and time points. An understanding of intensity tuning under these stimuli will require knowledge on more details of synaptic circuits, e.g., the origins and properties of presynaptic neurons for each synaptic input, that underlie cortical neurons' responses.

Experimental Procedures

Extracellular Recording

All experimental procedures used in this study were approved under the Animal Care and Use Committee at the University of Southern California. Experiments were carried out in a sound-proof booth (Acoustic Systems). Female Sprague-Dawley rats about 3 months old and weighing 250–300 g were anesthetized with ketamine and

xylazine (ketamine, 45 mg/kg; xylazine, 6.4 mg/kg; i.p.). The right auditory cortex was exposed, and the right ear canal was plugged. The body temperature was maintained at 37.5°C by a feedback heating system (Harvard Apparatus, MA). Multiunit spike responses were recorded with parylene-coated tungsten microelectrodes (FHC, ME) at 500–600 μm below the pial surface (Zhang et al., 2001; Bao et al., 2003; Polley et al., 2004). Electrode signals were amplified (Plexon Inc, TX), band-pass filtered between 300 and 6000 Hz, and then thresholded in custom-made software (LabView, National Instrument) to extract the spike times. Pure tones (0.5–64 kHz at 0.1 octave intervals, 25 ms duration, 3 ms ramp) at eight 10 dB spaced sound intensities were delivered through a calibrated free-field speaker facing the left ear. A time window from 10 to 25 ms from the onset of tone stimulus was used for tone-evoked spike responses. The threshold of the spike TRF was chosen to be the minimum stimulus intensity included in the TRF, and the characteristic frequency (CF) was the tone frequency that evoked a response at threshold. Bandwidth at 10 dB or 30 dB (BW10 or BW30) above threshold was the frequency width (in octaves) of the TRF at that intensity level. Auditory cortical mapping was carried out by sequentially recording from an array of cortical sites with an average grid size of 120 μm for dense mappings and about 200 μm for rough mappings (Kilgard and Merzenich, 1999; Zhang et al., 2001; Bao et al., 2003; Polley et al., 2004; Tan et al., 2004).

In Vivo Whole-Cell Recording

Whole-cell recordings (Moore and Nelson, 1998; Margrie et al., 2002; Zhang et al., 2003; Wehr and Zador, 2003; Tan et al., 2004) were obtained from neurons located 500–700 μm beneath the cortical surface. We prevented cortical pulsation with 4% agarose. For voltage-clamp recording, the patch pipette (4–7 M Ω) contained (in mM) 125 Cs-gluconate, 5 TEA-Cl, 4 MgATP, 0.3 GTP, 10 phosphocreatine, 10 HEPES, 0.5 EGTA, 2 CsCl, pH 7.2. QX-314 (5 mM) was included to improve the whole-cell clamping of the cell (Nelson et al., 1994). Recordings were made with an Axopatch 200B amplifier (Axon Instruments). The whole-cell recording method under our conditions shows a sampling bias toward relatively large pyramidal neurons, consistent with results from other laboratories with similar experimental settings (Moore and Nelson, 1998; Margrie et al., 2002). The whole-cell and pipette capacitances were completely compensated, and the initial series resistance (20–50 M Ω) was compensated for 50%–60% to achieve effective series resistances of 10–25 M Ω . Signals were filtered at 5 kHz and sampled at 10 kHz. Only neurons with resting membrane potentials lower than –55 mV and stable series resistance (less than 10% change from the beginning of the recording) were used for further analysis. The CFs of the synaptic TRFs of recorded neurons matched their positions in the tonotopic map determined by extracellular recordings.

Data Analysis

The excitatory synaptic conductance $G_e(t)$ and inhibitory synaptic conductance $G_i(t)$ at time t were derived (Borg-Graham et al., 1998; Anderson et al., 2000) using $I(t, V) = G_r(V - E_r) + G_e(t)(V - E_e) + G_i(t)(V - E_i)$, where V is the clamping voltage, G_r is the resting conductance, E_r is the resting potential, E_e and E_i are the reversal potentials for excitatory and inhibitory synaptic currents, respectively, and $I(t, V)$ is the current amplitude under V . Currents into the neuron were assigned a negative value. The resting or leak conductance G_r was derived using $I_r(V) = G_r(V - E_r)$, where E_r is the resting potential, and $I_r(V)$ is the resting current. Measurement of $I(V)$ at two voltages will solve the value of G_e and G_i in the equation. In this study, a corrected clamping voltage V was used, instead of the clamping voltage applied (V_c). $V(t)$ is given by $V(t) = V_c - R_s \times I(t)$, where R_s was the effective series resistance. Synaptic currents were obtained with the cell clamped at the reversal potentials for inhibitory and excitatory currents, respectively, for each of the 568 test tone stimuli. For some of the experiments, the reversal potentials of glutamatergic and GABAergic (Cl^-) currents were roughly measured at the beginning by examining the reversal of spontaneous glutamatergic and GABAergic currents, respectively, as the holding potential was changed. Under experimental condition in this study, the reversal potential was found to be 0–8 mV for glutamatergic inputs, and around –70 mV for GABAergic inputs, consistent with the values of E_e and E_i determined by considering the ionic composition of

the pipette solution and the cerebrospinal fluid. In some cases, E_r values of –65 and –75 mV were also tested, and this did not change the conclusion of the study.

Estimated membrane potential response V_{est} was simply derived from synaptic conductances using $V_{\text{est}}(t) = (G_r E_r + G_e(t) E_e + G_i(t) E_i) / (G_r + G_e(t) + G_i(t))$, where E_r is the resting membrane potential, which was determined for each recorded neuron under current-clamp recording at the beginning of the experiment. If only the excitatory synaptic conductance was taken into account, $G_i(t)$ was set to zero. The spike threshold was set around –45 mV for auditory cortical neurons, an observation from a previous study (Tan et al., 2004).

In this study, we have assumed linear, isopotential neurons in deriving excitatory and inhibitory synaptic conductances, same as in previous studies (Zhang et al., 2003; Wehr and Zador, 2003, 2005; Tan et al., 2004). However, deviations due to space-clamp error and cable attenuation for synaptic inputs at the distal dendrites (Spruston et al., 1993) should be kept in mind, as extensively discussed in several recent studies (Wehr and Zador, 2003; Tan et al., 2004). Nevertheless, the two major observations for intensity-tuned neurons, the nonmonotonic excitatory and monotonic inhibitory inputs as well as the nonmonotonic change of temporal delay between excitation and inhibition, are unlikely to be affected. First, the linearity of synaptic I-V curves (Figure 2E) suggested that synaptic conductances were not strongly affected by nonlinearities of cortical neurons. This may be attributed to the use of intracellular cesium, TEA, QX-314, and ketamine anesthesia, which together block most voltage-dependent currents. The relative accuracy of derived excitatory reversal potential (Figure 2E) also suggests reasonably accurate voltage-clamp for those recorded synaptic inputs, because errors in space-clamp will result in apparent deviations from the actual real reversal potential (Shu et al., 2003). In addition, the use of cesium and TEA (blockers of potassium channels) will reduce the membrane permeability and thus decrease the cable attenuation (Spruston et al., 1993). Second, we make comparisons between responses to CF stimuli in the same recorded cell and between intensity-tuned and nontuned neurons. Although space-clamp errors or cable attenuation will cause an underestimation of absolute conductances, our conclusions are not dependent on the absolute level of conductances or the ratio between excitation and inhibition. Finally, simulation based on a compartmental neuron model suggests that the relative timing between excitatory and inhibitory inputs at 50% peak is not significantly affected by the cable effects (Wehr and Zador, 2003).

Acknowledgments

We thank Dr. A.P. Sampath for helpful discussion. This work is supported by grants from NIH/NIDCD, Searle Scholar Program, Klingenstein Foundation, and National Organization for Hearing Research Foundation.

Received: May 19, 2006

Revised: August 28, 2006

Accepted: October 12, 2006

Published: November 21, 2006

References

- Anderson, J.S., Carandini, M., and Ferster, D. (2000). Orientation tuning of input conductance, excitation, and inhibition in cat primary visual cortex. *J. Neurophysiol.* 84, 909–926.
- Aitkin, L. (1991). Rate-level functions of neurons in the inferior colliculus of cats measured with the use of free-field sound stimuli. *J. Neurophysiol.* 65, 383–392.
- Aitkin, L.M., and Webster, W.R. (1972). Medial geniculate body of the cat: organization and responses to tonal stimuli of neurons in ventral division. *J. Neurophysiol.* 35, 365–380.
- Bao, S., Chang, E.F., Davis, J.D., Gobeske, K.T., and Merzenich, M.M. (2003). Progressive degradation and subsequent refinement of acoustic representations in the adult auditory cortex. *J. Neurosci.* 23, 10765–10775.

- Borg-Graham, L.J., Monier, C., and Fregnac, Y. (1998). Visual input evokes transient and strong shunting inhibition in visual cortical neurons. *Nature* 393, 369–373.
- Brudzynski, S.M., and Pniak, A. (2002). Social contacts and production of 50-kHz short ultrasonic calls in adult rats. *J. Comp. Psychol.* 116, 73–82.
- Brudzynski, S.M., Bihari, F., Ociepa, D., and Fu, X.W. (1993). Analysis of 22 kHz ultrasonic vocalization in laboratory rats: long and short calls. *Physiol. Behav.* 54, 215–221.
- Brugge, J.F., Dubrovsky, N.A., Aitkin, L.M., and Anderson, D.J. (1969). Sensitivity of single neurons in auditory cortex of cat to binaural tonal stimulation; effects of varying interaural time and intensity. *J. Neurophysiol.* 32, 1005–1024.
- Calford, M.B., and Semple, M.N. (1995). Monaural inhibition in cat auditory cortex. *J. Neurophysiol.* 73, 1876–1891.
- Cruikshank, S.J., Rose, H.J., and Metherate, R. (2002). Auditory thalamocortical synaptic transmission in vitro. *J. Neurophysiol.* 87, 361–384.
- Davies, P.W., Erulkar, S.D., and Rose, J.E. (1956). Single unit activity in the auditory cortex of the cat. *Bull. Johns Hopkins Hosp.* 99, 55–86.
- Doron, N.N., Ledoux, J.E., and Semple, M.N. (2002). Redefining the tonotopic core of rat auditory cortex: physiological evidence for a posterior field. *J. Comp. Neurol.* 453, 345–360.
- Evans, E.F., and Whitfield, I.C. (1964). Classification of unit responses in the auditory cortex of the unanesthetized and unrestrained cat. *J. Physiol.* 171, 476–493.
- Faingold, C.L., Boersma Anderson, C.A., and Caspary, D.M. (1991). Involvement of GABA in acoustically-evoked inhibition in inferior colliculus neurons. *Hear. Res.* 52, 201–216.
- Greenwood, D.D., and Maruyama, N. (1965). Excitatory and inhibitory response areas of auditory neurons in the cochlear nucleus. *J. Neurophysiol.* 28, 863–892.
- Hashimoto, H., Moritani, N., Aoki-Komori, S., Tanaka, M., and Saito, T.R. (2004). Comparison of ultrasonic vocalizations emitted by rodent pups. *Exp. Anim.* 53, 409–416.
- Heil, P. (2004). First-spike latency of auditory neurons revisited. *Curr. Opin. Neurobiol.* 14, 461–467.
- Heil, P., and Irvine, D.R. (1998). The posterior field P of cat auditory cortex: coding of envelope transients. *Cereb. Cortex* 8, 125–141.
- Heil, P., Rajan, R., and Irvine, D.R. (1994). Topographic representation of tone intensity along the isofrequency axis of cat primary auditory cortex. *Hear. Res.* 76, 188–202.
- Kalatsky, V.A., Polley, D.B., Merzenich, M.M., Schreiner, C.E., and Stryker, M.P. (2005). Fine functional organization of auditory cortex revealed by Fourier optical imaging. *Proc. Natl. Acad. Sci. USA* 102, 13325–13330.
- Kaltwasser, M.T. (1990). Acoustic signaling in the black rat (*Rattus rattus*). *J. Comp. Psychol.* 104, 227–232.
- Kaur, S., Lazar, R., and Metherate, R. (2004). Intracortical pathways determine breadth of subthreshold frequency receptive fields in primary auditory cortex. *J. Neurophysiol.* 91, 2551–2567.
- Kiang, N.Y., Watanabe, T., Thomas, E.C., and Clark, L.F. (1965). *Discharge Patterns of Single Fibers in the Cat's Auditory Nerve* (Cambridge, MA: MIT Press).
- Kilgard, M.P., and Merzenich, M.M. (1999). Distributed representation of spectral and temporal information in rat primary auditory cortex. *Hear. Res.* 134, 16–28.
- Kitzes, L.M., and Hollrigel, G.S. (1996). Response properties of units in the posterior auditory field deprived of input from the ipsilateral primary auditory cortex. *Hear. Res.* 100, 120–130.
- Kuwabara, N., and Suga, N. (1993). Delay lines and amplitude selectivity are created in subthalamic auditory nuclei: the brachium of the inferior colliculus of the mustached bat. *J. Neurophysiol.* 69, 1713–1724.
- Margrie, T.W., Brecht, M., and Sakmann, B. (2002). In vivo, low-resistance, whole-cell recordings from neurons in the anaesthetized and awake mammalian brain. *Pflügers Arch.* 444, 491–498.
- Miller, K.D., Pinto, D.J., and Simons, D.J. (2001). Processing in layer 4 of the neocortical circuit: new insights from visual and somatosensory cortex. *Curr. Opin. Neurobiol.* 11, 488–497.
- Moore, C.I., and Nelson, S.B. (1998). Spatio-temporal subthreshold receptive fields in the vibrissa representation of rat primary somatosensory cortex. *J. Neurophysiol.* 80, 2882–2892.
- Nelson, S., Toth, L., Sheth, B., and Sur, M. (1994). Orientation selectivity of cortical neurons during intracellular blockade of inhibition. *Science* 265, 774–777.
- Nyby, J., and Whitney, G. (1978). Ultrasonic communication of adult myomorph rodents. *Neurosci. Biobehav. Rev.* 2, 1–14.
- Ojima, H., and Murakami, K. (2002). Intracellular characterization of suppressive responses in supragranular pyramidal neurons of cat primary auditory cortex in vivo. *Cereb. Cortex* 12, 1079–1091.
- Phillips, D.P., and Kelly, J.B. (1989). Coding of tone-pulse amplitude by single neurons in auditory cortex of albino rats (*Rattus norvegicus*). *Hear. Res.* 37, 269–279.
- Phillips, D.P., and Orman, S.S. (1984). Responses of single neurons in posterior field of cat auditory cortex to tonal stimulation. *J. Neurophysiol.* 51, 147–163.
- Phillips, D.P., Semple, M.N., and Kitzes, L.M. (1995). Factors shaping the tone level sensitivity of single neurons in posterior field of cat auditory cortex. *J. Neurophysiol.* 73, 674–686.
- Pollak, G.D., and Park, T.J. (1993). The effects of GABAergic inhibition on monaural response properties of neurons in the mustache bat's inferior colliculus. *Hear. Res.* 65, 99–117.
- Polley, D.B., Heiser, M.A., Blake, D.T., Schreiner, C.E., and Merzenich, M.M. (2004). Associative learning shapes the neural code for stimulus magnitude in primary auditory cortex. *Proc. Natl. Acad. Sci. USA* 101, 16351–16356.
- Polley, D.B., Steinberg, E.E., and Merzenich, M.M. (2006). Perceptual learning directs auditory cortical map reorganization through top-down influences. *J. Neurosci.* 26, 4970–4982.
- Read, H.L., Winer, J.A., and Schreiner, C.E. (2002). Functional architecture of auditory cortex. *Curr. Opin. Neurobiol.* 12, 433–440.
- Rouiller, E., de Ribaupierre, Y., Morel, A., and de Ribaupierre, F. (1983). Intensity functions of single unit responses to tone in the medial geniculate body of cat. *Hear. Res.* 11, 235–247.
- Sales, G.D., and Pye, D. (1974). *Ultrasonic Communication by Animals* (London: Chapman and Hall).
- Schreiner, C.E., Mendelson, J.R., and Sutter, M.L. (1992). Functional topography of cat primary auditory cortex: representation of tone intensity. *Exp. Brain Res.* 92, 105–122.
- Shamma, S.A. (1985). Speech processing in the auditory system. II: Lateral inhibition and the central processing of speech evoked activity in the auditory nerve. *J. Acoust. Soc. Am.* 78, 1622–1632.
- Shu, Y., Hasenstaub, A., and McCormick, D.A. (2003). Turning on and off recurrent balanced cortical activity. *Nature* 423, 288–293.
- Sivaramakrishnan, S., Sterbing-D'Angelo, S.J., Filipovic, B., D'Angelo, W.R., Oliver, D.L., and Kuwada, S. (2004). GABA (A) synapses shape neuronal responses to sound intensity in the inferior colliculus. *J. Neurosci.* 24, 5031–5043.
- Spruston, N., Jaffe, D.B., Williams, S.H., and Johnston, D. (1993). Voltage- and space-clamp errors associated with the measurement of electrotonically remote synaptic events. *J. Neurophysiol.* 70, 781–802.
- Suga, N., and Manabe, T. (1982). Neural basis of amplitude-spectrum representation in auditory cortex of the mustached bat. *J. Neurophysiol.* 47, 225–255.
- Sutter, M.L., and Loftus, W.C. (2003). Excitatory and inhibitory intensity tuning in auditory cortex: evidence for multiple inhibitory mechanisms. *J. Neurophysiol.* 90, 2629–2647.
- Sutter, M.L., and Schreiner, C.E. (1995). Topography of intensity tuning in cat primary auditory cortex: single-neuron versus multiple-neuron recordings. *J. Neurophysiol.* 73, 190–204.
- Tan, A.Y., Zhang, L.I., Merzenich, M.M., and Schreiner, C.E. (2004). Tone-evoked excitatory and inhibitory synaptic conductances of primary auditory cortex neurons. *J. Neurophysiol.* 92, 630–643.

- Tan, A.Y., Atencio, C.A., Polley, D.B., Merzenich, M.M., and Schreiner, C.E. (2006). Unbalanced synaptic inhibition can create intensity-tuned auditory cortex neurons. Published online July 21, 2006. arXiv: q-bio.NC/0607036 21 Jul.
- Wang, J., McFadden, S.L., Caspary, D., and Salvi, R. (2002). Gamma-aminobutyric acid circuits shape response properties of auditory cortex neurons. *Brain Res.* 944, 219–231.
- Wehr, M., and Zador, A.M. (2003). Balanced inhibition underlies tuning and sharpens spike timing in auditory cortex. *Nature* 426, 442–446.
- Wehr, M., and Zador, A.M. (2005). Synaptic mechanisms of forward suppression in rat auditory cortex. *Neuron* 47, 437–445.
- Young, E.D., and Brownell, W.E. (1976). Response to tones and noise of single cells in dorsal cochlear nucleus of unanesthetized cats. *J. Neurophysiol.* 39, 282–300.
- Zhang, L.I., Bao, S., and Merzenich, M.M. (2001). Persistent and specific influences of early acoustic environments on primary auditory cortex. *Nat. Neurosci.* 4, 1123–1130.
- Zhang, L.I., Tan, A.Y., Schreiner, C.E., and Merzenich, M.M. (2003). Topography and synaptic shaping of direction selectivity in primary auditory cortex. *Nature* 424, 201–205.
- Zhu, Y., Stornetta, R.L., and Zhu, J.J. (2004). Chandelier cells control excessive cortical excitation: characteristics of whisker-evoked synaptic responses of layer 2/3 nonpyramidal and pyramidal neurons. *J. Neurosci.* 24, 5101–5108.